β-delayed neutron emission studies of ^{137,138}I and ^{144,145}Cs performed with trapped ions

A. Czeszumska, N. D. Scielzo, S. A. Caldwell, J. A. Clark, G. Savard, B. S. Wang, A. Aprahamian, M. T. Burkey, C. J. Chiara, J. Harker, A. F. Levand, S. T. Marley, G. Morgan, J. M. Munson, E. B. Norman, A. Nystrom, R. Orford, S. W. Padgett, A. Pérez Galván, K. S. Sharma, K. Siegl, and S. Y. Strauss

Phys. Rev. C **101**, 024312 — Published 26 February 2020

DOI: 10.1103/PhysRevC.101.024312

Beta-delayed neutron studies of ^{137,138}I and ^{144,145}Cs performed with trapped ions

A. Czeszumska,[1,2,*] N. D. Scielzo,[1] S. A. Caldwell,[3,†] J. A. Clark,[3] G. Savard,[3,4] B. S. Wang,[1,2] A. Aprahamian,[5] M. T. Burkey,[3,4] C. J. Chiara,[3,6,‡] J. Harker,[3,6] A. F. Levand,[3] S. T. Marley,[5] G. Morgan,[7] J. M. Munson,[2] E. B. Norman,[2] A. Nystrom,[5] R. Orford,[8,3] S. W. Padgett,[1] A. Pérez Galván,[3,§] K. S. Sharma,[7] K. Siegl,[5] and S. Y. Strauss[5]

[1]*Nuclear and Chemical Sciences Division, Lawrence Livermore National Laboratory, Livermore, California 94550, USA*
[2]*Department of Nuclear Engineering, University of California, Berkeley, California 94720, USA*
[3]*Physics Division, Argonne National Laboratory, Argonne, Illinois 60439, USA*
[4]*Department of Physics, University of Chicago, Chicago, Illinois 60637, USA*
[5]*Department of Physics, University of Notre Dame, Notre Dame, Indiana 46556, USA*
[6]*Department of Chemistry and Biochemistry, University of Maryland, College Park, Maryland 20742, USA*
[7]*Department of Physics and Astronomy, University of Manitoba, Winnipeg, Manitoba R3T 2N2, Canada*
[8]*Department of Physics, McGill University, Montréal, Québec H3A 2T8, Canada*

(Dated: January 21, 2020)

A detailed study of the β-delayed neutron emission properties of ^{137,138}I and ^{144,145}Cs has been performed by confining ions in the Beta-decay Paul Trap. The daughter ions following β decay emerge from the trapped-ion cloud with negligible scattering allowing reconstruction of the recoil-ion energy from the time-of-flight. From this information, the neutron-emission branching ratios and neutron-energy spectra were deduced. The results for the ^{137}I and ^{144,145}Cs decays are in agreement with previous results performed using direct neutron-detection techniques. In the case of ^{138}I, a branching ratio of 6.18(50)% is obtained, yielding a value consistent with the more recent results which are a factor of two larger than measurements made prior to 1978.

I. INTRODUCTION

For neutron-rich isotopes sufficiently far from stability, the β^--decay Q values become larger than the neutron separation energy, S_n, of the daughter nucleus. In these cases, the β decay may populate excited states above S_n which deexcite by neutron emission. This decay mode, known as β-delayed neutron (βn) emission, can become the dominant decay mode for isotopes sufficiently far from stability and therefore plays an important role in the understanding of nucleosynthesis and of the nuclear structure of neutron-rich nuclei. It is also important in applied nuclear physics [1] because it is energetically accessible for many fission products.

Roughly half of the isotopes of elements from iron to uranium are thought to be produced through repeated neutron-capture reactions and β decays in the rapid neutron-capture process (r process) [2, 3]. Beta-delayed neutron emission can significantly influence how the neutron-rich isotopes synthesized in r-process environments decay back to stability and provides an additional source of late-time neutrons. The resulting decay-chain shifts and subsequent late capture of these neutrons during freeze out can be substantial [4–6] and require better understanding. To date, there have been few measurements of delayed-neutron properties for isotopes near the proposed r-process path and sensitive techniques are needed to reach these exotic, short-lived isotopes.

Reviews of βn properties highlight that a detailed understanding of reactor kinetics and behavior under various accident and component-failure scenarios requires higher-quality nuclear data [1, 7]. Approximations suitable for light-water reactors that account for the differences in the delayed-neutron and fission-neutron energy spectra are likely not adequate for fast breeder reactors [8], necessitating more precise βn data [3]. Improved nuclear data would allow an accurately modeled delayed-neutron flux and energy spectrum for any fuel-cycle concept, actinide mix, or irradiation history.

High-quality βn measurements also provide constraints for nuclear-structure calculations [9] and phenomenological models [10–12] used to predict the decay properties for nuclei for which no data exist, as well as improve the accuracy and flexibility of the existing empirical descriptions of delayed neutrons such as the six-group representation [1]. Despite the importance of βn data, the existing nuclear data are limited, especially for the neutron-energy spectra, and some recent studies have revealed discrepancies in published neutron-emission branching ratios [13, 14].

The International Atomic Energy Agency (IAEA) has identified βn precursors in different mass regions that could serve as well-established "standards" for the purpose of data evaluation and measurement. For the heavy-mass peak of the fission-product distribution, the IAEA recommended the precursors ^{137}I and ^{138}I as standards. These isotopes are abundantly produced in the fission of actinides and therefore are important to nuclear-energy

* agac@berkeley.edu; Present address: mittemitte GmbH, Berlin, Germany
† Present address: Rigetti Computing, Berkeley, California 94710, USA
‡ Present address: U.S. Army Research Laboratory, Adelphi, Maryland 20783, USA
§ Present address: Vertex Pharmaceuticals, San Diego, California 92121, USA

applications. However, the IAEA cautioned that the ^{138}I evaluation was based on only two independent measurements, having excluded some discrepant results from prior to 1978 in their recommended value [15].

In the work presented here, the β decays of ^{137,138}I and ^{144,145}Cs ions were studied in detail using the Beta-decay Paul Trap (BPT) [16], an open-geometry linear radiofrequency quadrupole (RFQ) ion trap designed for precision β-decay studies. The ions were held in vacuum, and the emitted β particles, γ rays, and low-energy recoiling nuclei were detected in coincidence. The βn branching ratios and energy spectra were inferred from the time-of-flight (TOF) spectra of the recoil ions using the approaches first developed in Ref. [17].

The decay of ^{137}I had previously been studied using a variety of neutron-detection techniques and the most recent measurements have provided consistent results [18, 19]. The ^{144,145}Cs decays had been studied using proton-recoil proportional counters [18, 20] and although the branching ratios had been determined to a relative uncertainty of 5%, the βn energy spectra had only been measured once.

For the decay of ^{138}I, however, the most recent measurements yielded branching ratios of 5.56(22)% [18] and 5.32(20)% [21], respectively, which are a factor of two larger than the measurements performed prior to 1978 [22, 23]. Additional results, especially from a measurement technique with a different set of systematic effects, were therefore desired to shed light on this discrepancy.

II. MEASUREMENT APPROACH

The βn branching ratio and energy spectra of ^{137,138}I and ^{144,145}Cs were determined from the recoil energy imparted to the daughter ions following β decay. The BPT was used to collect and suspend radioactive ions in vacuum at the center of a radiation-detector array. The detector array consisted of two ΔE-E plastic scintillator telescopes, two microchannel plate (MCP) detectors, and two high-purity germanium (HPGe) detectors, used to detect the β particles, recoiling daughter ions, and γ rays, respectively, emitted following the decay. Figure 1 depicts the arrangement of the BPT and the detector array.

Following β decay, the recoil ions emerge from the trap volume essentially unperturbed by scattering. Decays for which a neutron has been emitted can be identified from the ions that have higher recoil energies than could be possible from the emission of only leptons and γ rays. Because the momentum imparted by an emitted neutron dominates the nuclear recoil, the neutron energy can be reconstructed using conservation of momentum. This novel way to perform βn spectroscopy circumvents the challenges associated with direct neutron detection.

The TOF of the recoiling ion is determined from the time difference between the detection of the β particle

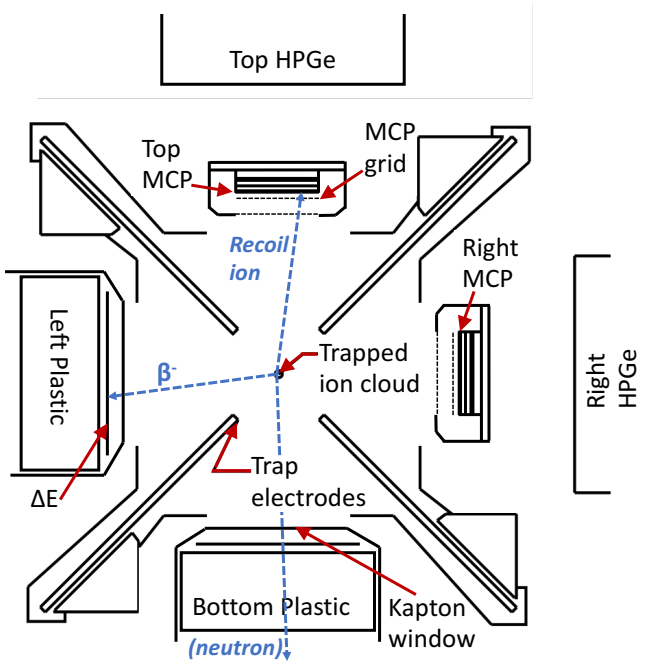

FIG. 1. (Color online) Schematic of the cross-sectional end view of the BPT experimental setup (not to scale). The dashed arrows represent an example of decay-product trajectories when a neutron is emitted.

and the associated recoiling daughter ion using thin ΔE plastic-scintillator detectors and MCP detectors, respectively. In the TOF spectrum, the higher-energy recoil ions characteristic of neutron emission (which have kinetic energies up to tens of keV) have shorter TOFs than the other recoiling daughter ions (which have kinetic energies less than 500 eV). The βn branching ratios can be deduced by comparing the number of β-ion coincidences with TOFs characteristic of neutron emission to the total number of β decays from trapped ions obtained from the number of detected: (1) β-ion coincidences with longer TOFs characteristic of β-decay to bound states, (2) β particles emitted from the trapped precursor, and (3) β-delayed γ rays. The agreement obtained for the βn branching ratios when using these three approaches provides additional confidence in the results.

III. EXPERIMENT

The βn precursors ^{137,138}I and ^{144,145}Cs were produced at the Californium Rare Isotope Breeder Upgrade (CARIBU) facility from the spontaneous fission of a $\approx$100-mCi ^{252}Cf source. The fission products emerging from the source were thermalized in helium buffer gas and extracted from the exit nozzle of the gas catcher [24] as primarily singly-charged ions using a combination of gas flow and electric fields. These ions were then focused into the RFQ section where the residual gas was pumped away and the ions were cooled and subsequently

accelerated to 36 keV for delivery to a high-resolution isobar separator [25]. The isobar separator was operated with a mass resolution of $M/\Delta M \approx$14000 to select a single mass-to-charge ratio. In the cases studied, there remained only a small contribution from the nearest-mass isobars, which was accounted for in the analysis.

The selected ions were then accumulated in an ion guide and delivered to the BPT in bunches, where the ions were captured, cooled, and trapped. The BPT electrodes consisted of four sets of stainless-steel plates which come within 11 mm of the trap center and are segmented into three sections along the beam axis. The radiofrequency (RF) voltages confined the ions radially, while the direct current (DC) potentials provided the axial confinement. The applied RF voltage was measured directly using a high-voltage probe following the data collection. The amplitude was determined to ±1% precision. The time-dependence was found to deviate slightly from $V_{RF}\cos(2\pi ft)$, with f=310 kHz, and $V_{RF} \approx$100 V, and could be described by including higher harmonics at 620 kHz and 930 kHz contributing with amplitudes less than 10% of the magnitude of the primary frequency. The trap stability condition, determined with the Mathieu equations [26], was selected such that the β-decay daughter ions, which all have a charge state of 2^+ or greater, were not confined in the trap. The DC potentials applied to the three sections along the beam axis were 20 V, −17 V, and 20 V. To cool the ions in the ion cloud, helium buffer gas (≈5x10^{-5} Torr) was injected into the center of the BPT.

Ions were accumulated in the BPT by maintaining a 5 V electrostatic valley at the center of the trap to retain the cold trapped-ion population while capturing a newly-delivered bunch. The accumulation periods ranged from 0.4 s for the ^{145}Cs measurement to as long as 6 s for the iodine isotopes. Following a fixed number of captures chosen for each nuclide, the trapped ions were ejected from the BPT and collected on a silicon detector about 1 m further downstream to monitor activity levels. The signals observed in the BPT detector array during the period after the ion-cloud ejection was used to assess backgrounds from outside the ion cloud. The number and length of the capture cycles and the length of the background measurements were chosen based on the radioactive half-life of the isotope being studied and the level of isobaric contamination. The average beam intensities for ^{137}I, ^{138}I, ^{144}Cs, and ^{145}Cs were about 800, 200, 600, and 100 ions/s, respectively.

The radiopurity of the beams was determined from the β particles and γ rays emitted from the trapped-ion samples. For each of the isotopes measured, the absence of the observation of any of the highest-intensity γ rays from the decay of the isobar closer to stability indicated that these isotopes contributed $< 1\%$ of the total trapped-ion activity. For the isobars further from stability, there was insufficient information on the γ-ray emission properties. In these cases, the time dependence of the buildup and decay of the β-particle detection rates over the course of the measurement cycle was used to determine the relative contributions because the half-life of the more exotic isobars was considerably shorter than the isotope under study. For ^{137}I, 20% of the trapped-ion decays were determined to have come from ^{137}Te, whereas for the other isotopes the time dependence was consistent with a pure beam of the isotope of interest. From this information, it was determined there was <10% of ^{138}Te and <2% of ^{144}Xe and ^{145}Xe in the ^{138}I, and ^{144}Cs and ^{145}Cs beams, respectively. For the more exotic neighboring isobars, these results were consistent with expectations based on the ^{252}Cf fission-product yield ratios relative to the isotope of interest. The beam content was also monitored periodically by performing mass analyses with the Canadian Penning Trap (CPT) mass spectrometer [27–29] to provide confirmation of the decay-counting results.

The β spectroscopy was performed with two ΔE-E detector telescopes made from EJ-204 plastic scintillator. Each detector consisted of a 1-mm-thick, 10.6-cm diameter ΔE detector positioned in front of a 10.2-cm-thick, 13.3-cm-diameter E detector capable of stopping the highest energy β particles from the fission-product decays. The ΔE detectors were located about 105 mm from the center of the BPT, and labeled as Left and Bottom in relation to their positions looking down the beam direction. The β particles were identified by energy deposition in the ΔE detector, as this thin detector has only a ≈1% intrinsic detection efficiency for γ rays and neutrons. The light from the ΔE detector was piped to two 1.5-inch diameter photomultiplier tubes (PMTs) using light-guide strips wrapped in thin specular reflectors. The E scintillator was coated in a layer of diffuse reflector paint and attached directly to a 5-inch diameter PMT. To prevent outgassing into the trap vacuum, each detector telescope was supported in its own vacuum chamber, separated from the ultrahigh-vacuum environment of the ion trap by a 10-μm-thick aluminized kapton window. The vacuum in the detector region was kept below 10^{-3} torr. Energy-deposition measurements from the conversion electrons from the ^{134}Sb isomer decay and from a spectroscopy-grade ^{207}Bi conversion-electron source indicated that the ΔE threshold for β particles was 76±24 keV and 62±30 keV for the Left and Bottom detectors, respectively.

Two resistive-anode Chevron-configured MCP detectors, each with a nominal active area of 50.3×50.3 mm^2, were used to detect recoil ions with 1-ns timing resolution. The MCP detectors, denoted as Right and Top to indicate their relative positions looking along the beam direction, were each located 53 mm from the trap center. The front face of the MCP detectors were biased to approximately −2.5 kV to accelerate the ions and improve the uniformity of the detection efficiency. Grounded, 89%-transmission grids situated 4.5 mm from the front face of the MCPs helped shield the detectors from the RF fields and prevented the MCP bias voltages from affecting the recoil-ion trajectories until the ions passed through the grid.

The relative amounts of charge collected at the four corners of the resistive anode allowed the determination of the ion impact position with sub-mm precision. The position calibration was established prior to data collection by observing the pattern that resulted from placing a mask on the surface of the MCP and illuminating it with a ^{238}Pu α-particle source. The entire MCP assembly was mounted on a ceramic plate, and covered with a grounded aluminum case with a square aperture covered by a second 89%-transmission grid. The MCP detector housings were specially designed to compactly fit between the electrodes of the BPT and to allow HPGe detectors to be brought within 10 cm of the trapped ion cloud.

Two coaxial single-crystal p-type HPGe detectors were mounted on the vacuum chamber in re-entrant ports. The Top detector was a 140%-relative-efficiency crystal, while the Right detector was a 80%-relative-efficiency crystal. The photopeak efficiencies were determined using ^{60}Co, ^{133}Ba, ^{137}Cs, and ^{152}Eu γ-ray sources with activities calibrated to 1.5–2.5% and a ^{56}Co source to extend the calibration up to 3.3 MeV. The sources were positioned within $\pm$1 mm of the geometric center of the trap using a specially-designed support mounted onto the RF electrodes.

Signal from any of the detectors triggered the data acquisition system by opening a 22-μs coincidence window for recording the amplitude and timing of the signals from each detector as well as the RF phase of the trap voltage. The deadtime per event was determined to be 142 μs.

Detailed Monte-Carlo simulations were used to interpret the results, calculate detection efficiencies, and determine systematic effects. The recoil-ion trajectories were calculated using SIMION 8.1 [30]. The Geant4 [31] simulation package was used to determine the energy deposition in the plastic-scintillator detectors from β particles, γ rays, neutrons, and conversion electrons. The β-decay kinematics were simulated using an event generator originally developed to study β-ν angular correlations [32, 33] and later adapted for βn emission [17] and complicated β-decay schemes [34, 35]. The decays were generated using an allowed β-decay energy spectrum and the known β-decay transitions to excited states in the daughter nucleus using data from NNDC [36] or from a simple model fit to the β-energy and recoil-ion TOF spectrum [35]. For βn emission, the β-ν angular correlation coefficient, $a_{\beta\nu}$, was assumed to be that of an allowed Gamow-Teller transition ($-1/3$). An additional "triple" correlation between the β, ν, and neutron can potentially arise [37] if the neutron is emitted with orbital angular momentum from the oriented β-decay daughter nucleus. The size of this correlation depends on the spins of the nuclear states involved in the β-decay and neutron-emission sequence. The transitions to many of the transitions to low-lying states, including the ground state, are first-forbidden so $a_{\beta\nu}$ is dependent on the matrix elements involved. For these transitions, an approximation was made that all β-decay branches for a given isotope have the same (initially unknown) value of $a_{\beta\nu}$. These properties were determined from an in-depth analysis of the β-ion coincidence data described in detail in Ref. [34, 35].

The simulation also took into account the charge-state distribution of the recoil ions and the size of the ion cloud. Analysis of the leading edge of the recoil-ion TOF distribution revealed that the ion-cloud spatial distribution was consistent with a Gaussian distribution of $\approx$1 mm [34] at full-width at half maximum (FWHM) when assumed to be identical in all three spatial dimensions. The charge-state distributions were estimated in Ref. [35] from the variation of the β-ion coincidence rate as a function of the phase of the RF voltage of the BPT using an approach described in detail in Ref. [34].

IV. NEUTRON ENERGY SPECTRA

The neutron energy E_n was deduced from the TOF of the recoil ion, t_{TOF}, and the hit position on the MCP surface which established the distance d traveled by the ion. The distance was approximated by a straight path from the trap center to the MCP grid, after which the ion acceleration into the MCP surface was calculated analytically. The value for t_{TOF} was also adjusted to account for the ion acceleration between the grid and the MCP surface. The E_n was then determined from the simple relation

$$E_n = \frac{M_r E_r}{m_n} = \frac{\frac{1}{2} M_r^2 (d/t_{TOF})^2}{m_n} \qquad (1)$$

where M_r and m_n are the masses of the recoil ion and the neutron, respectively, and E_r is the recoil-ion energy. Ultimately, an additional small correction for the lepton contribution to E_n was also included for coincidences involving back-to-back detector pairs.

The TOF of the recoil ions emerging from the BPT was used to identify the β decays which were followed by neutron emission. The TOF spectra for the decays of ^{137,138}I and ^{144,145}Cs are shown in Fig. 2. The βn decays give rise to a peak in the TOF spectrum that extends from about 0.3 μs out to about 1.6 μs, where it begins to overlap with β-ion coincidences recorded from β decays without accompanying neutron emission. The TOF distribution of the βn events was used to determine the neutron-energy spectrum. The narrow peak at 0 μs was from nearly-simultaneous coincidences of β particles and/or γ rays in the β detector and MCP detector and established the timing offset.

The largest recoil energy that can be imparted from the decays without neutron emission ranges from 166 eV following the decay of ^{137}I to 301 eV following the decay of ^{144}Cs. These values correspond to the recoil energy that would be imparted by the emission of 23–43-keV neutrons. These decays, if they occur at the center of the trap and result in a 2^+ daughter ion, could yield TOFs as short as 2.5–3.0 μs. As can be seen in Fig. 2, the TOF distribution of the events without neutron emission

peaks around 3–4 μs; however, the spread of the decay positions in the ion cloud and the impact the electric fields have on the motion of the daughter ions causes this TOF distribution to extend to less than about 2 μs. To ensure that βn decays were resolved from the other β decays, only events yielding reconstructed neutron energies of >100 keV, corresponding to events with TOFs less than 1.6–1.7 μs, were attributed to βn emission.

The neutron-energy calibration is dependent on the distance between the center of the ion cloud and the MCP detector. This distance was determined to be 53.0(5) mm for both MCP detectors from a detailed analysis of the recoil-ion TOF spectrum following the β decay of ^{134}Sb [34]. These results were consistent with the distances of 52.5(3) mm and 52.9(3) mm determined from physical measurements of the placement of the detectors and electrodes. The value obtained from the recoil-ion TOF spectrum is used in the analysis and results in a 2% uncertainty in the energy determination. The neutron-energy resolution varies with energy from 30-50 keV at the lowest neutron energies to 100-150 keV FWHM at 1 MeV (depending on the isotope). The resolution is largely determined by the 1-mm FWHM spatial extent of the ion cloud and the additional recoil imparted by the leptons. The neutron-energy spectrum determined from the β-ion coincidences requires accounting for a number of backgrounds, efficiency factors, as well as energy shifts which arise from the recoil imparted by the leptons. The following subsections examine these effects in detail.

A. Backgrounds

The random-coincidence rate was determined from the ΔE-MCP detector coincidences between 15 and 20 μs, a region devoid of true β-ion coincidences as indicated by both data and simulations. After accounting for the accidental coincidences, an excess of ΔE-MCP coincidences at TOFs less than 1 μs was still present in the TOF spectrum recorded when the trap was purposefully held empty and was likely due to the short-lived activity that accumulated on the BPT or detector surfaces over the course of the measurements. This background was most pronounced between 50–200 ns and decreased with increasing TOF; however, it extended into the TOF region where the recoil ions from βn emission were observed. A similar excess of counts at TOFs shorter than 200 ns was also evident in the spectra collected with trapped ions. In order to determine the background present at TOFs longer than 200 ns when trapped ions were present, the characteristic TOF distribution observed without trapped ions was scaled based on the number of counts observed between 50–200 ns. This background accounted for between 7 and 11% of the counts in the βn TOF region for ^{137,138}I and ^{145}Cs. For ^{144}Cs, the correction was a larger fraction of the coincidences at 31%, because of the smaller branching ratio for βn emission.

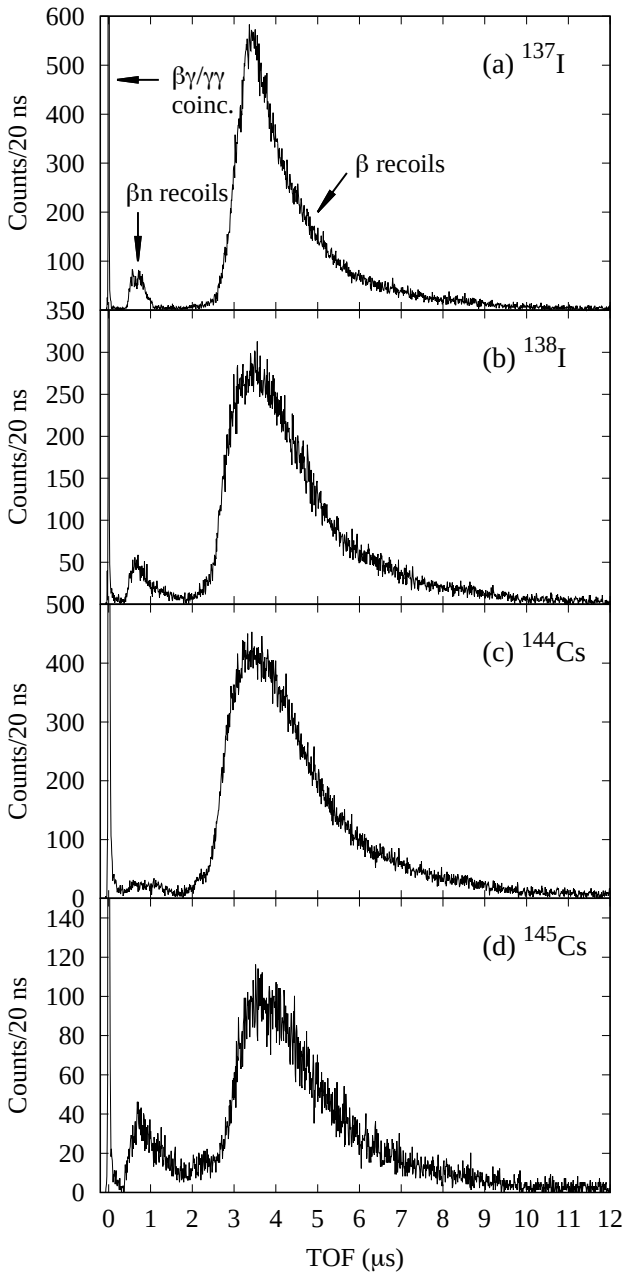

FIG. 2. Recoil-ion TOF spectra following the β decay of a) ^{137}I, b) ^{138}I, c) ^{144}Cs, and d) ^{145}Cs. Each spectrum shows the sum of the four ΔE-MCP detector combinations after the subtraction of random coincidences. The coincidences between 0.3 and 1.6 μs are due to recoil ions having emitted a neutron, whereas the vast majority of the distribution beyond 2 μs is due to decays without neutron emission. For ^{137}I decays, the TOF distribution beyond 2 μs is narrower than the others primarily because the large transition strength to the ground state and the correlation between the leptons lead to the recoil-ion momenta distribution being more focused opposite the β-particle momentum.

B. Lepton-recoil energy shift

The neutron energy determined using Eq. 1 neglects the momentum imparted to the nucleus from the lepton emission. For β-ion coincidences detected with the ΔE-MCP detector pair separated by 180°, the β-particle momentum is roughly in the same direction as the neutron momentum. Therefore, on average this effect increases the energy of the nuclear recoil, although the size of the shift is influenced by both the β-ν angular correlation and the triple correlation. As a result, the neutron energy inferred using Eq. 1, which attributes the entire recoil energy to the neutron, results in an overestimation of the neutron energy. The correction applied to the reconstructed neutron-energy spectrum was estimated by comparing the energies of simulated neutrons emitted following β decay to the energies reconstructed from the interpretation of the recoil-ion TOF.

Without including the triple correlation, the energy shift for the 180° detector pair was determined to be ≈15% for 100-keV neutrons, decreasing to below 2% for neutrons with energies above 1000 keV. For the 90° detector pair, the β momentum is roughly orthogonal to the neutron momentum, and its impact on the recoil energy was found to be negligible.

The inclusion of the triple correlation modifies this lepton-recoil energy shift, as it impacts the distribution of neutrino momenta associated with detected β-ion coincidences. The magnitude of the triple correlation depends on the spins of the nuclear states involved in the decay sequence and the orbital angular momentum L of the neutron relative to the nucleus. The impact of this additional correlation was minor — regardless of the details of the decay, its presence could change the calculated energy shift from the lepton recoil by less than a quarter of its size. Here, it was assumed that neutron emission was dominated by the spin sequence which yielded the lowest L for the emitted neutron. For ^{138}I, ^{144}Cs, and ^{145}Cs, a L=0 transition is accessible, and the resulting triple-correlation coefficient is zero. For ^{137}I, a L=2 transition was the lowest accessible, and the resulting correlation increased the energy shift by about 20% of the value obtained without it (or typically about 5 keV and <1 keV for the 180° and 90° detector pair, respectively) across all energies.

C. Neutron-ion coincidences

The momentum of the neutron is nearly in the opposite direction of the recoil-ion momentum so the neutron likely intercepts the ΔE detector opposite the MCP detector struck by the recoil ion. As a result, neutron-ion coincidences can yield an additional ≈10% ΔE-MCP coincidences for the detector pair separated by 180°, despite the small intrinsic detection efficiency for neutrons. The response of plastic scintillators to neutrons, which is mediated through proton recoil, typically induces a roughly 5 times smaller light yield than β particles depositing the same energy [38]. Since these neutron-ion coincidences could not be distinguished from β-ion coincidences, they increased the total coincidence detection efficiency for the 180° detector pair.

The neutron detection threshold for the ΔE detectors was estimated from the measured ratio of ΔE-ΔE-MCP triple coincidences (which are expected to be predominantly from β-neutron-ion coincidences) to the ΔE-MCP coincidences. The neutron detection threshold in the simulation was adjusted until it best matched the experimental results for the isotopes studied here. The resulting neutron-detection threshold of 370(70) keV was consistent with the factor of 5 less scintillation light expected for neutrons compared to β particles.

D. MCP detector efficiency

The intrinsic detection efficiency of MCP detectors is nearly independent of energy for keV-energy heavy ions [39]. However, a small ion-impact-energy dependence can arise because a fraction of recoils with lower energies produce a signal below the electronic threshold [39, 40]. Due to the Poisson nature of the electron-multiplication process in MCP detectors [41], the pulse-height distribution (PHD) from ion-impact events can be described by a Gaussian distribution [42] with the centroid and standard deviation both dependent on the detector gain and the impact energy of the ion [39]. The centroid of the PHD was observed to increase linearly with the impact energy, which is consistent with the Parilis-Kishinevskii relation [43], while the width of the PHD was observed to be independent of the ion-impact energy. The detector gain was found to vary somewhat over the fiducial area of the MCP. To account for this spatial variation, the MCP was subdivided into 16 square regions and the PHD from each region was then separately fit to determine the parameters for the Gaussian distribution. Figure 3 shows the measured PHD and resulting model fit for the entire MCP detector for the lowest-energy ions (the ions resulting from decays without neutron emission) which have the lowest centroid and therefore show the largest fraction of events below the threshold. Following an approach similar to the one used in Ref. [42], the fraction of counts above the discriminator threshold was calculated analytically from the established relationship between the ion-impact velocity and the PHD gain. The results are shown in Fig. 4. The Top MCP detector had a significantly lower gain than the Right MCP detector, resulting in a decreased detection efficiency, especially for the lowest-energy recoil ions. The analysis of the MCP detector efficiency is described in detail in Ref. [44].

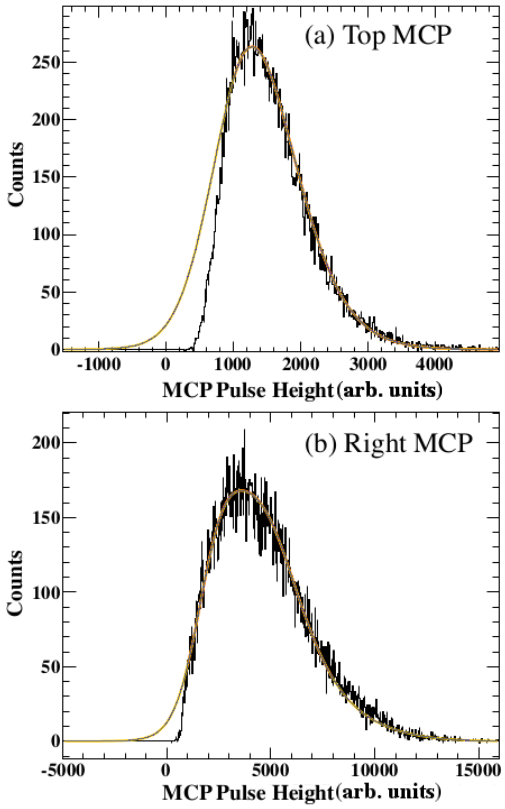

FIG. 3. (Color online) The PHD for ^{137}Xe ions following the β decay of ^{137}I striking the (a) Top and (b) Right MCP detectors with impact energies of 5 keV. The fit (shown as smooth line in yellow (light-grey)) is a sum of Gaussian distributions which take into account the observed spatial variation in gain across the face of the MCP detector. This gain variation imparts a visible skew to the PHD. The spectra for the other isotopes are similar.

E. Coincidence detection efficiency

The likelihood of both a β particle and a recoil ion following β decay striking ΔE and MCP detectors, respectively, and generating pulses large enough to rise above the detector thresholds depends on the decay kinematics and therefore varies with the neutron energy. The scattering of β particles off the electrodes and other material within the chamber increases the β-particle detection efficiency by up to 30% above what would be expected from the detector solid angle alone. For β particles, the detection efficiency is affected by the energy loss in the thin kapton window in front of the plastic detector and the ΔE detector threshold. The ion trajectories, and therefore fraction of ions striking an MCP detector, is affected by the RF and DC fields. The MCP energy-dependent efficiency correction and the neutron-ion coincidence correction, discussed earlier, also influence the total coincidence detection efficiency. Figure 5 shows the total β-ion coincidence detection efficiency for each ΔE-MCP detector pair for the case of ^{137}I decay, expressed as a fraction by normalizing it to the product of the corresponding detector solid angles. The β-ν and triple correlations, regardless of their size, have a negligible impact on the resulting efficiency.

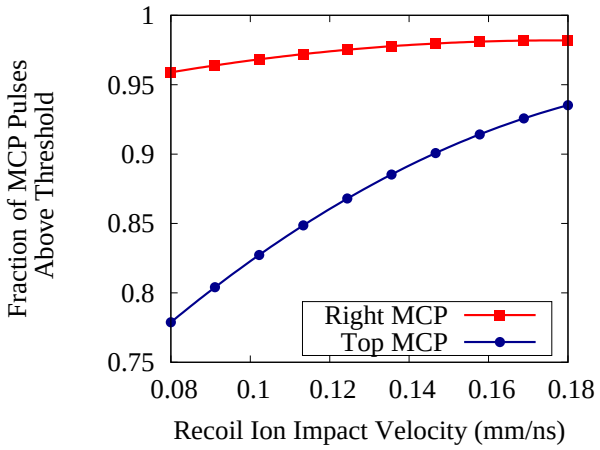

FIG. 4. (Color online) The calculated fraction of MCP detector pulses above the discriminator threshold as a function of ion-impact velocity. The recoil ions from β decays to the ground state or accompanied by γ-ray emission have impact velocities around 0.08 mm/ns, whereas recoil ions following βn emission have a range of energies that extend well above 0.10 mm/ns.

The resulting neutron-energy spectra for ^{137,138}I and ^{144,145}Cs determined from the recoil-ion TOF spectra are shown in Fig. 6 and are compared to previous results that were directly measured using ^{3}He ionization chambers (^{137}I [45] and ^{138}I [46]), and proportional counters (^{138}I [47] and ^{144,145}Cs [20]). In each case, the results confirm the existing measurements in the energy range above 100 keV. Below 100 keV, the βn recoils cannot be distinguished from the other recoil ions and therefore no information about the βn energy spectrum was obtained. The results obtained with the BPT are subject to different systematic effects than encountered using conventional direct neutron detection techniques. Direct measurements are typically affected by large backgrounds from scattered neutrons and γ rays, and require applying spectral unfolding due to the detector response [1, 48, 49]. These challenges are lessened in the recoil-ion technique, since the line shape of the reconstructed energy is nearly Gaussian without a low-energy tail and there are few backgrounds that are present at the TOFs corresponding to the recoiling ions.

V. BETA-DELAYED NEUTRON BRANCHING RATIOS

For each isotope, the βn branching ratio, P_n, was determined from the ratio of the detected number of β-ion co-

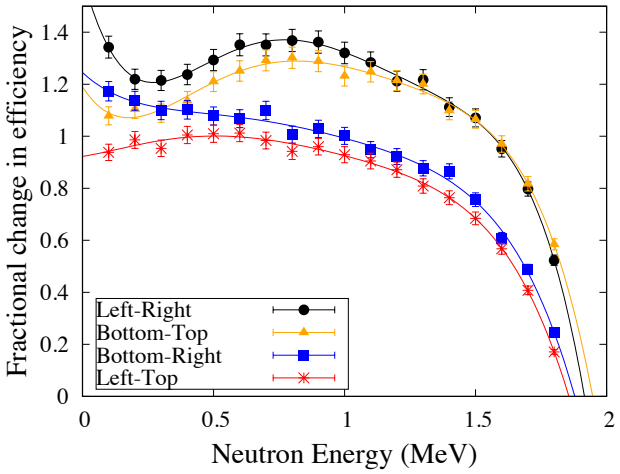

FIG. 5. (Color online) The coincident β-ion detection efficiency (normalized to the product of the corresponding detector solid angles, and hence expressed as a fraction) for the βn decay of ^{137}I for each ΔE-MCP detector pair. The 180° detector combinations have higher efficiencies primarily due to the additional contribution from neutrons triggering the ΔE detector in coincidence with the recoiling ion. For the highest neutron energies, little energy remains for the leptons, and therefore the fraction of β particles detected drops rapidly; although this effect is large for decays populating excited states within 500 keV of $Q_\beta - S_n$, a negligible fraction of the neutron spectrum is typically found there due to the highly suppressed phase space for these decays. The lower efficiency of the Top MCP detector is also evident. The detection-efficiency curves for the other isotopes show similar features and also only begin a rapid drop within 500 keV of $Q_\beta - S_n$.

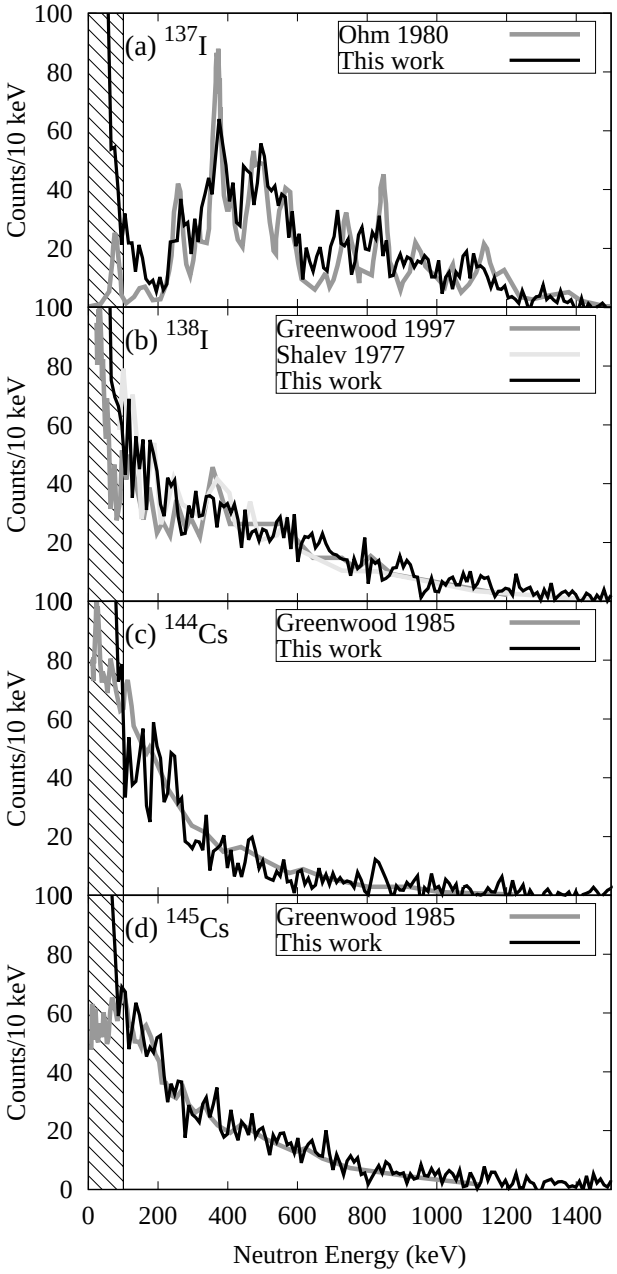

FIG. 6. Neutron-energy spectra determined from β-ion coincidences compared to previous results from direct neutron-detection methods: Shalev 1977: [46], Greenwood 1997: [47], and Greenwood 1985: [20]. In the region filled with hatch lines, the βn decays cannot be resolved from decays without neutron emission.

incidences with TOF characteristic of βn emission, $n_{\beta R}$, to the total number of detected β decays, after taking into account the efficiency for detecting these decay signatures. The total number of detected β decays were determined in three different ways, through the number of detected (1) β-ion coincidences with longer TOFs characteristic of lepton and γ-ray emission, $n_{\beta r}$, (2) β particles originating from the trapped species of interest, n_β, and (3) β-γ-ray coincidences, $n_{\beta\gamma}$. In the following equations, R and r denote recoils from β decay with and without neutron emission, respectively.

In each case, the results obtained with each ΔE-MCP coincidence pair were analyzed separately because of their different detection efficiencies and then averaged to determine P_n for that method.

A. P_n obtained from the recoil-ion TOF spectrum

The P_n for each isotope can be determined solely from the recoil-ion TOF spectrum, by taking the ratio of the number of βn events to the total number of recoil ions from β decay with and without neutron emission:

$$P_n = \frac{\frac{n_{\beta R}}{\epsilon_{\beta R}\cdot f}}{\frac{n_{\beta R}}{\epsilon_{\beta R}\cdot f} + \frac{n_{\beta r}}{\epsilon_{\beta r}}} = \frac{n_{\beta R}}{n_{\beta R} + n_{\beta r}\frac{\epsilon_{\beta R}\cdot f}{\epsilon_{\beta r}}} \quad (2)$$

where $\epsilon_{\beta R}$ is the detection efficiency for the β-ion coincidences characteristic of neutron emission, $\epsilon_{\beta r}$ is the β-ion coincident detection efficiency for the recoil ions without neutron emission, and f is the fraction of the neutron-energy spectrum above a threshold of 100 keV, for which the recoil-ion energies could be unambiguously identified as being from neutron emission. The values for f were determined from previous direct measurements of the neutron-energy spectra [20, 45–47] and were 0.96(1), 0.81(5), 0.69(4), and 0.76(3) for ^{137}I, ^{138}I, ^{144}Cs, and ^{145}Cs, respectively.

The advantage of determining P_n solely from the recoil-ion TOF spectrum is that the intrinsic efficiency of the MCP detector cancels out in the ratio $\epsilon_{\beta R}/\epsilon_{\beta r}$ after taking into account the impact of the detection threshold as discussed in Section IV D. The $\epsilon_{\beta R}$ values for each ΔE-MCP detector pair were obtained from the efficiency curves used in interpreting the neutron-energy spectrum, analogous to the ones shown in Fig. 5. However, determining $\epsilon_{\beta r}$ is challenging because the recoil ions have energies less than 500 eV and are significantly perturbed by the electric fields of the BPT. Hence, $\epsilon_{\beta r}$ is sensitive to the details of the decay scheme, as well as the charge-state distribution of the recoil ions following the β decay.

The decay information needed to determine $\epsilon_{\beta r}$ includes the charge-state distribution of the recoiling ions, the β intensities and β-ν angular correlations for each transition, and the corresponding γ-ray cascades. The β-decay and γ-ray-cascade information is typically either incomplete or unavailable. However, $\epsilon_{\beta r}$ could be estimated using the data collected in the experiment by adjusting decay-scheme parameters until both the β-energy distribution and the ratio of measured β-ion coincidences at 180° and 90° detector pairs were reproduced by the simulation. As demonstrated in Ref. [35], this method determines the fraction of ions which reach the MCP detector to a precision of within ±4%, allowing the ratio $\epsilon_{\beta r}/\epsilon_{\beta R}$ to be determined to a precision of ±7%. The P_n values obtained from the recoil-ion TOF spectrum are listed in Table I.

B. P_n obtained from β-particle detection

By comparing $n_{\beta R}$ to the number of detected β particles, P_n can also be determined from

$$P_n = \frac{n_{\beta R}}{n_\beta} \cdot \frac{\epsilon_\beta}{\epsilon_{\beta R}} \cdot \frac{1}{f}, \tag{3}$$

where ϵ_β is the β-particle detection efficiency.

To determine n_β, the fraction of total ΔE triggers originating from the trapped species of interest had to be isolated from the background from any neighboring isobars and any activity located outside of the ion cloud. This was accomplished by comparing the data to a model that takes into account the buildup and decay of the different species over the course of the measurement cycle while enforcing the decay-feeding relationships between different populations [50]. The time dependence of the β-particle signal rate over the course of the measurement cycle was sufficient to determine n_β to better than 5% precision in all cases.

	P_n (%)			
Method	^{137}I	^{138}I	^{144}Cs	^{145}Cs
βr	7.18(56)	6.18(50)	2.95(24)	13.53(90)
β	6.13(49)	5.82(55)	2.49(23)	13.15(104)
$\beta\gamma$	7.16(96)	6.34(86)	2.31(36)	16.84(279)

TABLE I. Summary of the P_n results obtained with the BPT. The results were determined by comparing the β-ion coincidences associated with βn emission to the detected β particles originating from the trapped species of interest ("β"), β-ion coincidences with longer TOFs characteristic of lepton and γ-ray emission ("βr"), and β-γ-ray coincidences ("$\beta\gamma$"). The value determined from the ratio of β-ion coincidences in the TOF spectrum (βr) is the recommended P_n

The values of ϵ_β were determined for each isotope from simulations that take into account the β-decay transitions and subsequent deexcitation cascades, the geometry of the ion trap and detector array, and the detector thresholds [36].

The intrinsic efficiency of the MCP detector influences $\epsilon_{\beta R}$ and was determined from a detailed study of the decay of trapped ^{134}Sb ions [34]. ^{134}Sb decays predominantly to the ground state of ^{134}Te via a first-forbidden 0^- to 0^+ transition, for which $a_{\beta\nu}$ is expected to be $\approx$1 [51]. By comparing the results from the simulation to the data, the MCP detector intrinsic efficiency (which includes the ion loss in passing through the two 89%-transmission grids) was determined to be 29.3(14)% for the Top MCP, and 33.3(15)% for the Right MCP. The resulting P_n values are summarized in Table I.

C. β-γ coincidences

The detection of characteristic γ rays in coincidence with the emitted β particle provided an additional way to determine the number of β decays from trapped ions. These β-γ coincidences were free from contributions from isobaric contaminants, because the energy of the γ-ray transitions are unique for each isotope. This enabled the βn branching ratio to be determined from

$$P_n = \frac{n_{\beta R}}{n_{\beta\gamma}} \cdot \frac{\epsilon_{\beta\gamma}}{\epsilon_{\beta R} \cdot I_\gamma \cdot f}, \tag{4}$$

where I_γ is the absolute intensity of the γ-ray transition and $\epsilon_{\beta\gamma}$ is the coincident detection efficiency for the β particles and the associated γ ray used to identify the decay of the nucleus of interest. Decays which occurred outside of the ion cloud contributed a β-γ coincidence background which had to be estimated from the data collected during the time after the ion cloud was ejected

Isotope	γ energy (keV)	I_γ(%)
^{137}I	1218.0, 1220.0	16.3(16)
^{137}Te	243.4	–
^{138}I	588.8	56.0(54)
^{138}Xe	258.1	31.5(13)
^{144}Cs	198.9	46.5(25)
^{144}Ba	387.9	13.4(13)
^{145}Cs	175.2	19.8(24)
^{145}Ba	544.3	9.9(12)

TABLE II. The γ-ray transitions and intensities (I_γ) used to characterize isobaric contaminants through the analysis of β-γ coincidence data. The values of I_γ used for each isotope were obtained from Ref. [36] except for ^{144}Cs which was from Ref. [52]. In the decay of ^{137}I, the two γ-ray lines listed were not resolved, so the sum was used. No γ-ray transitions are known for the decay of ^{144}Xe and ^{145}Xe. The absolute intensity of the γ-ray transition following ^{137}Te β decay is also not known.

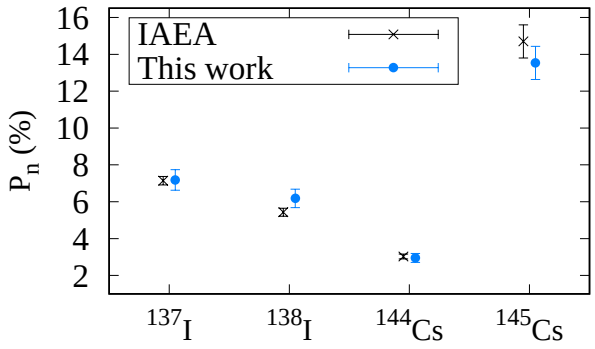

FIG. 7. (Color online) Comparison of the BPT results (βr P_n values) to the recommended IAEA values [15] obtained from previous direct measurements.

and the trap held empty. In the case of ^{137}I, the feeding from the decay of ^{137}Te also had to be taken into account. The P_n results obtained using Eq. 4 are summarized in Table I and have relative uncertainties of about 15–20%. The γ rays and I_γ values used are listed in Table II; the uncertainties on this available nuclear data were typically 10% or greater. In addition, the statistical precision obtained for $n_{\beta\gamma}$ was limited primarily because ε_γ was less than 1% for each HPGe detector.

D. Discussion of the P_n results

The P_n values obtained for ^{137,138}I and ^{144,145}Cs are summarized in Table I. These results utilized auxiliary measurements of the neutron-energy spectrum to account for the fraction of the spectrum below 100 keV that was unobserved. For each isotope, the three methods yielded consistent values, and the highest fractional precision was obtained from the results obtained solely from the recoil-ion TOF spectrum. Determining P_n from a ratio of β-ion coincidences has the advantage that it involves the same detectors and coincidence requirements and the efficiency ratio $\epsilon_{\beta R}/\epsilon_{\beta r}$ can be accurately determined. Therefore, the recommended P_n values for each isotope from this work are from the β-ion coincidence ratio — the agreement of the other measurement approaches serves as important confirmation of these results.

The results obtained with the BPT are compared to the IAEA evaluations in Fig. 7. In each case, the results agree well with the values recommended by the IAEA which are an evaluated world average of the previous measurements. The results for ^{138}I are of particular interest as the most recent measurements [18, 21] indicated the P_n is a factor of two larger than the results obtained from earlier measurements [22, 23]. As a result, the IAEA evaluation had been based solely on the two most recent results, leading them to warn this standard should be used with caution. The results obtained using the BPT are consistent with the recent measurements and provide confidence that the earlier values are discrepant and should be excluded from the evaluated average. The comparison of the P_n value obtained here with the results from previous experiments is shown in Fig. 8. The values in Refs. [22, 23] were determined by separately measuring β particles and neutrons from ^{238}U and ^{232}Th fission products, a method that relies on accurate assessment of the total β activity and hence is subject to uncertainty from improperly-subtracted contaminants. Furthermore, the older data were normalized to now-obsolete fission yields. Now that there are three independent measurements for ^{138}I that are in agreement, this should greatly increase the confidence of using this isotope as a reliable standard.

VI. CONCLUSIONS AND OUTLOOK

The βn branching ratios and energy spectra for ^{137,138}I and ^{144,145}Cs βn precursors were determined by studying the momentum distribution of the recoiling ions following β decay. The measurements presented here for ^{137,138}I and ^{144,145}Cs were carried out by delivering mass-separated beams from the CARIBU facility to the BPT where the activity was collected and held in vacuum. Following β decay within the trapped ion cloud, the emitted β particles, γ rays, and low-energy recoiling ions emerged with minimal scattering and βn emission branching ratios and energy distributions were inferred from the recoils imparted to the nuclei. The measurements performed with trapped ions allow three methods to determine P_n by detecting the β particles, recoiling ions, and γ rays in coincidence. Each of these approaches is subject to different systematic uncertainties and yields consistent results with an uncertainty of about 10-20%. The method of obtaining P_n directly from the ratio of β-ion coincidences

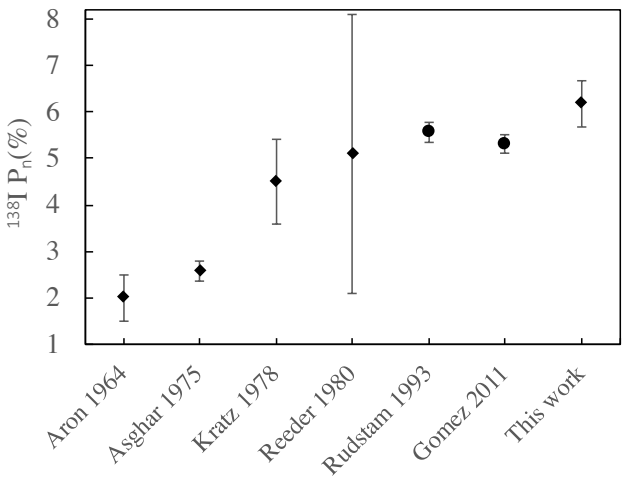

FIG. 8. Comparison of ^{138}I P_n values from Aron 64: [22], Asghar 1975: [23], Kratz 1978: [53], Reeder 1980: [19], Rudstam 1993: [18], and Gomez 2011: [21] with the results from this work (using the βr P_n value).

is unique to this ion-trap method and yields the highest precision result because many of the systematic uncertainties associated with the coincident detection cancel. This approach of studying βn emission allows measurement of both the energy spectrum and the branching ratio in the same experiment and is subject to different systematic effects than direct neutron detection experiments.

The results for ^{137}I and ^{144,145}Cs obtained here are consistent with previous measurements employing direct neutron detection. The results for ^{138}I confirm the more recent P_n measurements and put the βn decay data for this nucleus on firmer footing. This should reduce concerns about ^{138}I serving as an IAEA standard, as consistent βn-decay properties have now been established through the use of several independent measurement techniques.

Additional upgrades to the experimental setup can be implemented to increase the solid-angle coverage of the detector array and to improve the ion collection and cooling while minimizing the effect of the electric fields on the recoil ions. Larger β and MCP detectors can increase the β-ion coincident detection efficiency by roughly a factor of four. Future experiments will also benefit from increases in the intensity and purity of the low-energy beams delivered by the CARIBU facility [54, 55]; there has been an order-of-magnitude increase in CARIBU beam intensities since these data were collected. Additional refinements to the electrode structure, such as bringing the electrodes closer to the ion trap center, should allow the use of lower-amplitude RF voltages, which will reduce the perturbation of the ion trajectories prior to reaching the MCP detectors. These improvements will allow measurements to probe more neutron-rich isotopes, where the data are scarce, and the decay properties will provide valuable information on r-process nucleosynthesis and the structure of nuclei far from stability.

ACKNOWLEDGMENTS

The assistance of the ATLAS staff is acknowledged and appreciated. This material is based upon work supported by the Department of Energy, NNSA, under Award Numbers DE-NA0000979 (NSSC), DE-AC52-07NA27344 (LLNL), and DE-NA0002135 (SSGF), Office of Nuclear Physics Contract DE-AC02-06CH11357 (ANL), NEUP Project Number 13-5485, and Grants DE-FG02-94ER40834 (University of Maryland), NSERC, Canada, under Application No. 216974, NSF contract PHY-1713857 (Notre Dame Nuclear Science Laboratory), and the Department of Homeland Security. A. C. acknowledges support from the Lawrence Scholar Program at LLNL.

[1] S. Das, Prog. Nucl. Energ. **28**, 209 (1994).
[2] E. M. Burbidge, G. R. Burbidge, W. A. Fowler, and F. Hoyle, Rev. Mod. Phys. **29**, 547 (1957).
[3] K.-L. Kratz, K. Farouqi, and B. Pfeiffer, Prog. Part. Nucl. Phys. **59**, 147 (2007).
[4] B. Pfeiffer, K.-L. Kratz, F.-K. Thielemann, and W. Walters, Nucl. Phys. A **693**, 282 (2001).
[5] K. Farouqi, K.-L. Kratz, B. Pfeiffer, T. Rauscher, F.-K. Thielemann, and J. W. Truran, Astrophys. J. **712**, 1359 (2010).
[6] M. Mumpower, R. Surman, G. McLaughlin, and A. Aprahamian, Prog. Part. Nucl. Phys. **86**, 86 (2016).
[7] R. Q. Wright and R. E. MacFarlane, Comp. Phys. Eng. **1** (2008).
[8] O. Sorlin and M.-G. Porquet, Prog. Part. Nucl. Phys. **61**, 602 (2008).
[9] T. Kawano, P. Möller, and W. B. Wilson, Phys. Rev. C **78**, 054601 (2008).
[10] E. A. McCutchan, A. A. Sonzogni, T. D. Johnson, D. Abriola, M. Birch, and B. Singh, Phys. Rev. C **86**, 041305 (2012).
[11] K. Miernik, Phys. Rev. C **88**, 041301 (2013).
[12] K. Miernik, Phys. Rev. C **90**, 054306 (2014).
[13] J. A. Winger, S. V. Ilyushkin, K. P. Rykaczewski, C. J. Gross, J. C. Batchelder, C. Goodin, R. Grzywacz, J. H. Hamilton, A. Korgul, W. Królas, *et al.*, Phys. Rev. Lett. **102**, 142502 (2009).
[14] P. Hosmer, H. Schatz, A. Aprahamian, O. Arndt, R. R. C. Clement, A. Estrade, K. Farouqi, K.-L. Kratz, S. N. Liddick, A. F. Lisetskiy, *et al.*, Phys. Rev. C **82**, 025806 (2010).
[15] D. Abriola, B. Singh, and I. Dillmann, *Summary Report*

of Consultants' Meeting on Beta-delayed neutron emission evaluation, Tech. Rep. INDC(NDS)-0599 (International Atomic Energy Agency, Vienna International Centre, Vienna, Austria, 2011).
[16] N. Scielzo, G. Li, M. Sternberg, G. Savard, P. Bertone, F. Buchinger, S. Caldwell, J. Clark, J. Crawford, C. Deibel, *et al.*, Nucl. Instr. Meth. Phys. Res. A **681**, 94 (2012).
[17] R. M. Yee, N. D. Scielzo, P. F. Bertone, F. Buchinger, S. Caldwell, J. A. Clark, C. M. Deibel, J. Fallis, J. P. Greene, S. Gulick, *et al.*, Phys. Rev. Lett. **110**, 092501 (2013).
[18] G. Rudstam, K. Aleklett, and L. Sihver, At. Data and Nucl. Data Tables **53**, 1 (1993).
[19] P. L. Reeder and R. A. Warner, *Delayed Neutron Emission Probabilities of Rb and Cs Precursors Measured by Both Ion and Beta Counting Techniques*, Tech. Rep. PNL-SA-8766 (Pacific Northwest Laboratory, 1980).
[20] R. C. Greenwood and A. J. Caffrey, Nucl. Sci. Eng. **91**, 305 (1985).
[21] M. B. Gómez-Hornillos, J. Rissanen, J. L. Taín, A. Algora, D. Cano-Ott, J. Agramunt, V. Gorlychev, R. Caballero, T. Martínez, L. Achouri, *et al.*, J. Phys. Conf. Ser. **312**, 052008 (2011).
[22] P. M. Aron *et al.*, Sovt. J. At. Energy **16**, 447 (1964).
[23] M. Asghar, J. P. Gautheron, G. Bailleul, J. P. Bocquet, J. Greif, H. Schrader, G. Siegert, C. Ristori, J. Crancon, and G. I. Crawford, Nucl. Phys. A **247**, 359 (1975).
[24] G. Savard, J. Clark, C. Boudreau, F. Buchinger, J. Crawford, H. Geissel, J. Greene, S. Gulick, A. Heinz, J. Lee, *et al.*, Nucl. Instr. Meth. Phys. Res. B **204**, 582 (2003).
[25] C. N. Davids and D. Peterson, Nucl. Instr. Meth. Phys. Res. B **266**, 4449 (2008).
[26] W. Paul, Rev. Mod. Phys. **62**, 531 (1990).
[27] G. Savard, R. C. Barber, D. Beeching, F. Buchinger, J. Crawford, S. Gulick, X. Feng, E. Hagberg, J. C. Hardy, V. T. Koslowsky, *et al.*, Nucl. Phys. A **626**, 353 (1997).
[28] J. C. Wang, G. Savard, K. S. Sharma, J. A. Clark, Z. Zhou, A. F. Levand, C. Boudreau, F. Buchinger, J. E. Crawford, J. P. Greene, *et al.*, Nucl. Phys. A **746**, 651 (2004).
[29] J. Van Schelt, D. Lascar, G. Savard, J. A. Clark, P. F. Bertone, S. Caldwell, A. Chaudhuri, A. F. Levand, G. Li, G. E. Morgan, *et al.*, Phys. Rev. Lett. **111**, 061102 (2013).
[30] D. Manura, Scientific Instrument Services, Inc. (2006-2008).
[31] S. Agostinelli *et al.*, Nucl. Instr. Meth. Phys. Res. A **506**, 250 (2003).
[32] N. D. Scielzo, S. J. Freedman, B. K. Fujikawa, and P. A. Vetter, Phys. Rev. A **68**, 022716 (2003).
[33] N. D. Scielzo, S. J. Freedman, B. K. Fujikawa, and P. A. Vetter, Phys. Rev. Lett. **93**, 102501 (2004).
[34] K. Siegl, N. D. Scielzo, A. Czeszumska, J. A. Clark, G. Savard, A. Aprahamian, S. A. Caldwell, B. S. Alan, M. T. Burkey, C. J. Chiara, *et al.*, Phys. Rev. C **97**, 035504 (2018).
[35] J. M. Munson, K. Siegl, N. D. Scielzo, B. S. Alan, A. Czeszumska, G. Savard, A. Aprahamian, S. A. Caldwell, C. J. Chiara, Clark, *et al.*, Nucl. Instrum. Methods Phys. Res., Sect. A **898**, 60 (2018).
[36] M. B. Chadwick, M. Herman, P. Obložinský, M. Dunn, Y. Danon, A. Kahler, D. Smith, B. Pritychenko, G. Arbanas, R. Arcilla, *et al.*, Nucl. Data Sheets **112**, 2887 (2011), special issue on ENDF/B-VII.1 Library.
[37] B. R. Holstein, Rev. Mod. Phys. **46**, 789 (1974).
[38] R. L. Craun and D. L. Smith, Nucl. Instrum. and Methods **80**, 239 (1970).
[39] G. W. Fraser, Int. J. Mass Spectrom. **215**, 13 (2002).
[40] S. Yagi, T. Nagata, M. Koide, Y. Itoh, T. Koizumi, and Y. Azuma, Nucl. Instr. Meth. Phys. Res. B **183**, 476 (2001).
[41] J. Oberheide, P. Wilhelms, and M. Zimmer, Meas. Sci. Technol. **8**, 351 (1997).
[42] E. Liénard, M. Herbane, G. Ban, G. Darius, P. Delahaye, D. Durand, X. Fléchard, M. Labalme, F. Mauger, A. Mery, *et al.*, Nucl. Instr. Meth. Phys. Res. A **551**, 375 (2005).
[43] E. S. Parilis and L. M. Kishinevskii, Sov. Phys. Solid State **3**, 885 (1960).
[44] A. Czeszumska, Ph.D. thesis, University of California, Berkeley, Department of Nuclear Engineering (2016).
[45] H. Ohm, M. Zendel, S. G. Prussin, W. Rudolph, A. Schröder, K.-L. Kratz, C. Ristori, J. A. Pinston, E. Monnand, F. Schussler, *et al.*, Z. Phys. A **296**, 23 (1980).
[46] S. Shalev and G. Rudstam, Nucl. Phys. A **275**, 76 (1977).
[47] R. C. Greenwood and K. D. Watts, Nucl. Sci. Eng. **126**, 324 (1997).
[48] H. Franz, W. Rudolph, H. Ohm, K.-L. Kratz, G. Herrmann, F. Nuh, D. Slaughter, and S. Prussin, Nucl. Instrum. Methods **144**, 253 (1977).
[49] K.-H. Beimer, G. Nyman, and O. Tengblad, Nucl. Instrum. Methods Phys. Res., Sect. A **245**, 402 (1986).
[50] S. A. Caldwell, Ph.D. thesis, University of Chicago, Department of Physics (2015).
[51] C. S. Wu and S. A. Moszkowski, *Beta Decay* (Interscience Publishers, New York, 1966).
[52] G. Rudstam, *Absolute gamma branching ratios for fission-products in the mass range 74-165*, Tech. Rep. INDC(SHD)-024 (The Studsvik Neutron Research Laboratory, Nykoping, Sweden, 1993).
[53] K.-L. Kratz, Radiochim. Acta **25**, 1 (1978).
[54] T. Y. Hirsh, N. Paul, M. Burkey, A. Aprahamian, F. Buchinger, S. Caldwell, J. A. Clark, A. F. Levand, L. L. Ying, S. T. Marley, *et al.*, Nucl. Instrum. Methods Phys. Res., Sect. B **376**, 229 (2016).
[55] G. Savard, A. Levand, and B. Zabransky, Nucl. Instrum. Methods Phys. Res., Sect. B **376**, 246 (2016).